Appendix A. Analytical model of gridded impacts of environmental constraints

In the base version of the model, regional crop prices are allowed to deviate from the world price according to the constant elasticity of substitution between domestic and world crops. However, we will also explore a hypothetical alternative in which commodity markets are fully integrated, so that there is a single crop price, worldwide. Both irrigated and rainfed production are subject to zero profit conditions, which implies that the percentage change in national output price must equal the cost share-weighted percentage changes of gridded input prices (Equations 1 and 2). Cost shares may vary by grid-cell, as well as by irrigation regime.

The model assumes that crop production follows a nested CES function (Figure S1), with inputs grouped into land and other non-land factors. The derived demand for agricultural inputs is determined by the change in output, the relative price of inputs, as well as the substitution between land and non-land inputs (Equations 3, 6, 7, and 9). Irrigated sector produces from other non-land inputs and a bundled land-water composite, in which irrigation water and irrigated land are treated as complementary (non-substituting) inputs. Rainfed sector produce crops using potentially irrigable but not irrigated land, and non-irrigable land. The secondary nesting in the production structure determines the derived demand for different types of land and water, again based on the CES production function.

The supply of non-land inputs is determined at the national level, as a function of the price of inputs and their respective supply elasticity (Equation 5). Land inputs contain two types of land, namely irrigable and non-irrigable land. Each has its own supply schedule due to the difference in land rents. Non-irrigable land is only supplied to rainfed crop production. Irrigable land in the model is split into two categories – already irrigated and potentially irrigable but not irrigated. The former is used by irrigated sectors, while the later enters the production nest of rainfed sectors. The supplies of irrigable and non-irrigable land are determined by the grid cell-specific land rents and the corresponding land supply elasticity (Equations 12 and 18). Total irrigable land is distributed to irrigated (irrigated) and rainfed sectors (irrigable but not irrigated) by a constant elasticity of transformation function (Equations 8 and 10), by assuming that irrigable land in rainfed sectors can be converted into irrigated land in irrigated sectors if irrigation is equipped in the area.

The national commodity market is cleared at the equilibrium commodity price. The factor market clearing condition determines the input prices for rainfed and irrigated land, water, and other non-land-water inputs at the grid-, hydrological sub-basin- and the political regional-level, respectively. Equation 19 determines the change of regional output, which is aggregated from the change at the grid-level. See Appendix B for data details.

(1) $po + ao = \theta_g^{iLand} p_g^{iLand} + (1-\theta_g^{iLand}) p^{nLand}$	: zero profits for irrigated crop sector in grid *g*
(2) $po + ao = \theta_g^{rLand} p_g^{rLand} + (1-\theta_g^{rLand}) p^{nLand}$	: zero profits for rainfed crop sector in grid *g*
(3) $q_g^{nLand} = \sum_j \beta_j^{nLand} \left[qo_{g,j} - ao - \sigma_{g,j} (p_{g,j}^{nLand} - po) \right], j = irr, rfd$	: grid-level demand for non-land inputs by irrigated and rainfed crops
(4) $q^{nLand} = \sum_{g \in reg} \beta_g^{nLand} q_g^{nLand}$	: regional demand for non-land inputs by irrigated and rainfed crops
(5) $q^{nLand} = \nu^{nLand} p^{nLand}$	: regional supply of non-land inputs to crop sectors
(6) $q_g^{LW} = qo_{g,irr} - ao - \sigma_{g,LW} (p_g^{LW} - po - ao)$	: grid-level demand for land-water composite by irrigated crop
(7) $q_{g,irr}^{iLand} = q_g^{LW} - \sigma_{g,iL} (p_{g,irr}^{Land} - p_g^{LW})$	: grid-level demand for **irrigated** land by irrigated crop
(8) $q_{g,irr}^{iLand} = q_{g,irr}^{Land} - \zeta_g (p_{g,irr}^{iLand} - p_{g,irr}^{Land})$	: grid-level supply of **irrigated** land to irrigated crop
(9) $q_{g,rfd}^{iLand} = q_{g,rfd}^{Land} - \sigma_{g,rL} (p_{g,rfd}^{iLand} - p_{g,rfd}^{Land})$	: grid-level demand for **irrigable** land by rainfed crop
(10) $q_{g,rfd}^{iLand} = q_{g,irr}^{Land} - \zeta_g (p_{g,rfd}^{iLand} - p_{g,irr}^{Land})$	: grid-level supply of **irrigable** land to rainfed crop
(11) $p_{g,irr}^{Land} = \sum_j \xi_{g,j}^{iLand} p_{g,j}^{iLand}, j = irr, rfd$	: grid-level demand for **irrigable** land to irrigated and rainfed crops
(12) $q_{g,irr}^{Land} = \nu_{g,irr}^{Land} p_{g,irr}^{Land}$	: grid-level supply of **irrigable** land to irrigated and rainfed crops
(13) $q_g^{Water} = q_g^{LW} - \sigma_{g,iL} (p_g^{Water} - p_g^{LW})$	: grid-level demand for irrigation water by irrigated crop
(14) $q_g^{Water} = \nu^{Water} (p_g^{Water} + \lambda_B)$	: grid-level supply of irrigation water to irrigated crop
(15) $q_B^{Water} = \sum_{g \in B} \gamma_g q_g^{Water}$	: sub-basin level demand for water by irrigated crop
(16) $q_{g,rfd}^{Land} = qo_{g,rfd} - ao - \sigma_{g,R} (p_{g,rfd}^{Land} - po)$	: grid-level demand for (**irrigable and non-irrigable**) land by rainfed crops
(17) $q_{g,rfd}^{rLand} = q_{g,rfd}^{Land} - \sigma_{g,rL} (p_g^{rLand} - p_{g,rfd}^{Land})$	: grid-level demand for **non-irrigable** land by rainfed crop
(18) $q_{g,rfd}^{rLand} = \nu_{g,rfd}^{Land} p_{g,rfd}^{rLand}$	: grid-level supply of **non-irrigable** land to rainfed crop
(19) $qo = \sum_g \sum_j \alpha_{g,j} qo_{g,j}, j = irr, rfd$	: regional crop output

Notation for analytical model.

qo : % change in crop output

q : % change in demand for agricultural input

po : % change in national price of agricultural output

p_g^X : % change in the price of agricultural input X

θ^{iLand} : cost share of irrigated land input in grid g

θ^{rLand} : cost share of rainfed land input in grid g

$\alpha_{g,j}$: national output share of crop j grown in grid g

ao : input-neutral efficiency index in crop sectors

γ_g : share of grid g water demand in sub-basin B

λ_B : shadow price of irrigation water in sub-basin B

$\sigma_{g,LW} \geq 0$: elasticity of substitution between land-water composite and non-land input in irrigated sector, grid g

$\sigma_{g,R} \geq 0$: elasticity of substitution between land and non-land inputs in rainfed sector, grid g

$\sigma_{g,iL} \geq 0$: elasticity of substitution between irrigated land and water, in irrigated sector, grid g

$\sigma_{g,rL} \geq 0$: elasticity of substitution between irrigable and non-irrigable land in rainfed sector, grid g

$\xi_{g,j}^{iLand} \geq 0, j = irr, rfd$: share of irrigated land in irrigated sector (if j=irr) and share of irrigable land in rainfed sector (if j=rfd), grid g

$\zeta_g < 0$: transformation elasticity between irrigated land and irrigable land in the CET nest of irrigable land, grid g

---

$\nu_{g,j}^{Land} \geq 0, j = irr, rfd$: elasticity of irrigated land supply (if j=irr) and non-irrigable land supply (if j=rfd), grid g

$\nu^{nLand} \geq 0$: elasticity of non-land input supply in the region

$\nu^{Water} \geq 0$: elasticity of irrigation water supply in the region

β_g^{nLand} : share of grid g non-land input in regional total

β_j^{nLand} : share of crop j non-land input, grid g

Appendix B. Description of data used in SIMPLE-on-a-Grid model, model coupling, and experiments

B.1. *Data details for SIMPLE and SIMPLE-on-a-Grid.*

National scale data and parameters are inherited from the *SIMPLE* model (Baldos and Hertel, 2013). Specifically, information on GDP (in constant 2000 USD) and population are extracted from the World Development Indicators (2015) and from the World Population Prospects (2015). Data on cropland cover, crop production, crop utilization, and crop prices are obtained from FAOSTAT (2014). The amount of crop feedstock used by biofuel sector is proportionate to total crop output, using the sale shares provided in the GTAP-BIO v.6 database. Shares constructed from FAOSTAT's crop utilization statistics are used to split the remaining crop quantities into other uses, namely food, feed, and raw material for processed food.

Several additional data sources are involved in the specification of *SIMPLE-on-a-Grid*. The share of irrigated land and output at the grids follows the Monthly Growing Area Grids (MGAG) data for 26 crops (Portmann et al., 2010). Before computing the aggregated shares, all crop outputs are converted to corn-equivalent values by weighting the output of crop k (in tons) by the price of crop k relative to corn in the base period. Using these shares, the initial value of regional land and output are downscaled to grid cells, and split into rainfed and irrigated categories. The grid-level irrigation water consumption (cubic meters per hectare) is computed as the ratio of blue water requirement to irrigated area, using data from the Global Crop Water Model (GCWM) supplied by Siebert and Döll (2010). Blue water is defined as the amount of productively or unproductively evapotranspiring water originating from river segments, aquifers, lakes and reservoirs, as opposed to the "green" part of soil water that originates directly from precipitation. By computing daily soil water balances, GCWM determines evapotranspiration of blue water for each crop and grid cell.

B.2. *Hydro-econ link*

Grid-cell level irrigation supply is determined by the price of water and a water supply elasticity, while the sub-basin level irrigation availability is restricted by the amount of residual water after non-crop water use has been satisfied. Specifically, sub-basin level water available for irrigation is computed as the sum of surface water flows, reservoir water, and shallow groundwater water, and then subtract total water withdrawals for residential, industrial and livestock uses. Each of these components is simulated by the WBM and then water available for irrigation at each sub-basin is passed to SIMPLE-on-a-Grid model (Figure B1).

Grid-cell level irrigation water demand is determined by a grid-level consumptive irrigation water use parameter and the endogenous demand for irrigated land simulated by SIMPLE-on-a-Grid model (as described in Appendix A). This irrigation water consumption, combined with the availability of irrigation water, is used to construct the irrigation vulnerability index.

Domestic and industrial water demand time series (1980-2099) were generated by applying a projected growth rate to the baseline year water withdrawal. The baseline national domestic and industrial water withdrawal data were extracted from FAO AQUASTAT data (FAO, 2016). The sources of these data originated from several different years centered around 2010, which we assume to be the base year for hydrological projections. In the absence of efficiency improvements in water use, domestic water demand grows faster than does population, reflecting that water use per capita increases as consumers become wealthier. According to a review by Nauges and Whittington (2010), the income elasticity of water demand is typically in the range 0.1-0.3. We adopt the midpoint value of 0.2 in this study. In other words, the demand for domestic water is expected to grow at a rate of population growth plus one-fifth of the growth rate of per capita GDP. Annual population and per capita GDP growth rate was computed from the IIASA population and GDP decadal projections (IIASA, 2007) under the B2 scenario, which assumes medium level of population and GDP growth and technological change by 2100 (see Appendix D for details). B2 scenario is also similar to RCP8.5 in terms of climate impacts.

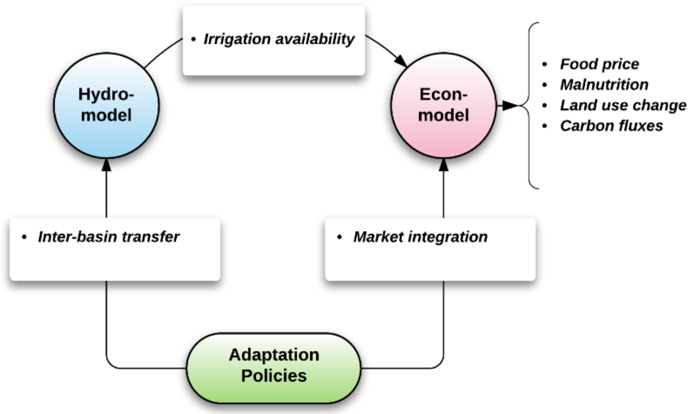

Figure B1. Hydrological model and economic model is linked at the sub-basin level by water available for irrigation.

B.3. *Description of experiments*

The baseline data for 2006 is first simulated forward to 2050 (the upper level dashed-line boxes in Figure B2) using exogenous shocks to population (UN Population Division, 2015), per capita income growth (Fouré et al., 2013; *World Development Indicators*, 2015), biofuels demand (IEA, 2008, 2012), as well as future TFP growth for crops, livestock, and processed food (Evenson and Gollin, 2003; Fuglie et al., 2007; Griffith et al., 2004; Ludena et al., 2007). For an extended analysis of global projections of crop output, land use and price, the reader is referred to Hertel, Baldos and van der Mensbrugghe (2016). These factors together determine the demand for irrigation water.

Next, irrigation vulnerability index is computed at the sub-basin level to determine the magnitude of sustainability shock. If the resulting index is greater than 0.2, the sustainability experiment shocks the 2050 baseline index such that no more than 20% of the total water available for irrigation at each sub-basin is consumed in the sustainable equilibrium (the lower level solid-line boxes in Figure B2). This procedure is then repeated under two assumptions on future TFP growth rate in irrigated sectors, namely equally fast or faster than that in rainfed sector.

Such an experimental design yields six sets of results in total: either equal or faster irrigated TFP growth interacted with business-as-usual as well as the two adaptations – inter-basin water transfer and integrated world markets. The water transfer experiment integrates sub-basins which are planned to be connected by large-scale hydro-projects. Water demand and supply are equalized at the integrated basin level, rather than at each individual sub-basin level. In the integrated market experiment, crop commodities are sold at the same price on all the markets. This, admittedly stylized assumption, provides a marked contrast to the way agricultural markets currently function, and yields markedly different pattern of regional crop supplies in 2050 (Hertel and Baldos, 2016). While we don't expect agricultural markets to be fully integrated in 2050, this allows us to evaluate the likely way in which a continued trend towards globalization would alter our baseline findings.

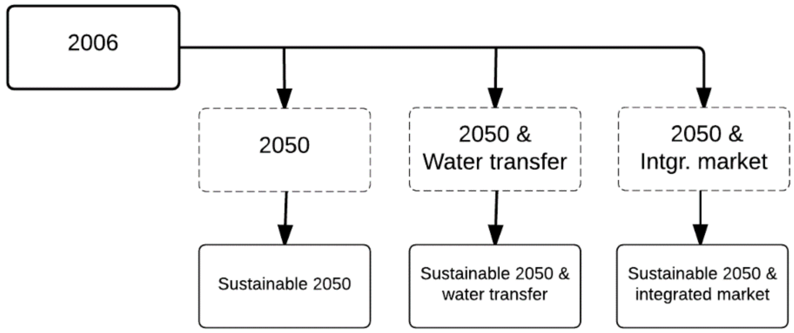

Figure B2. Experimental design.

Appendix C. WBM model

C.1. *WBM description*

WBM is a grid-based hydrology model used to simulate and track water fluxes and balances between atmosphere, above-ground water storages (e.g. snowpack, glaciers, others), soil, vegetation (including crops), groundwater, runoff, and water transport in streams and stream storages along many choices of river networks, hydro-infrastructure units (e.g. reservoirs, connectivity canals, etc.), and a number anthropogenic water usages such as irrigation, domestic, industrial demands, and others. The fundamental formulations for water balance processes used in its algorithm come from many physical hydrology studies summarized in (Dingman, 2002) and specifically applied to hydrological cycle modeling that comprised the earlier versions of WBM for global modeling of mostly pristine environments (Federer et al., 2003; Rawlins et al., 2003; Vörösmarty et al., 1998). The more recent development of WBM expanded its modeling framework to many anthropogenic interactions with hydrological cycle such as coupling biogeochemical (Wollheim et al., 2008), hydro-infrastructure engineering (Wisser et al., 2008, 2013), interbasin water transfer (Zaveri et al., 2016), irrigation (Grogan, 2016; Wisser et al., 2010), agricultural land use (Grogan et al., 2015), water use regulations (Murphy et al., 2014, 2015), and many other human impacts on surface water hydrology (Vörösmarty et al., 2010).

Full documentation for WBM can be found in (D. Wisser et al., 2010; Grogan, 2016).

C.2. *Model Inputs*

Table D1: Input datasets used for WBM simulations

Input Data	**Source**
Digital river network	STN-30p, global[a]
ET model, and open water evaporation model	Hamon and Dingman[b]
Soil and active layer properties	Harmonized Soil Map[c]
Impervious surfaces	NOAA NGCD[d]
Rainfed and irrigated crop map and crop parameters	MIRCA-2000[e]
Dam and reservoir hydro-infrastructure database	GRanD[f]
climate drivers	
Air temperature at 2 m, historical	NASA MERRA[g]
Precipitation, historical	NASA MERRA[g]
Specific/relative humidity	NASA MERRA[g]
Wind speed at 10 m	NASA MERRA[g]
Precipitation daily downscaling (for future)	GPCP[h]
Air temperature at 2 m, future	GISS-E2-R, RCP 8.5[i]
Precipitation, future	GISS-E2-R, RCP 8.5[i]

[a]Vörösmarty et al., 2000
[b]Dingman, 2002; Hamon, 1963
[c]FAO/IIASA/ISRIC/ISS-CAS/JRC, 2009

[d]Elvidge et al., 2007
[e]Portmann et al., 2010
[f]Lehner et al., 2011
[g]Global Modeling and Assimilation Office (GMAO), 2011
[h]Huffman et al., 2001
[i]Schmidt et al., 2014

Note on future climate inputs: For this simulation, the GISS-E2-R (Schmidt et al., 2014) air temperature and precipitation projections were bias corrected and downscaled using the delta change method. The bias correction factors were calculated by comparing the historical GISS-E2-R simulated monthly climatologies to the NASA MERRA (Global Modeling and Assimilation Office (GMAO), 2011) monthly climatologies. WBM runs on a daily time step; the monthly precipitation values were downscaled to daily values using a distribution of precipitation patterns from the GPCP (Huffman et al., 2001) observed climate product, and average daily temperatures were assumed to be constant through the month.

C.3. *Inter-basin Transfers*

WBM simulates transfers of water between hydrologic basins by moving water across basin divides from one river location to another (Zaveri et al., 2016). We simulate both existing inter-basin transfers - transfers with infrastructure that was completed prior to 2006 – and future potential transfers. Future potential transfers were determined by literature review of government and NGO proposals. For all inter-basin transfers (completed and proposed), five parameters are used to simulate the transfer. These are: the donor/from latitude and longitude, the recipient/to latitude and longitude, a minimum allowed flow, a maximum allowed flow, and a rule for flow volumes between the minimum and. In some cases, maximum allowed flow is based on published reported annual transfer capacities. In addition to the reported latitudes and longitudes of the transfers, we grid cell based locations for each transfer, which in some cases are different than the reported location because they were adjusted to ensure they linked to the correct rivers within the STN-30p network version 6.02. The completed transfers were implemented in the year that construction was completed; proposed transfers are turned on at their proposed completion date, as there is no set date for completing construction of these transfers.

The volume of water transferred through each canal is calculated as:

$$D = \begin{cases} 0 & if\ Q_d \leq Q_{min} \\ (Q_d - Q_{min}) * \frac{P}{100} & if\ Q_{min} > \ Q_d \geq Q_{max} \\ Q_{max} & if\ Q_d > Q_{max} \end{cases} \quad (10)$$

where D [m^{3}s^{-1}] is the amount of water diverted through the canal, Q_d [m^{3}s^{-1}] is the donor river discharge, Q_{min} [m^{3}s^{-1}] is the minimum flow parameter, Q_{max} [m^{3}s^{-1}] is the maximum flow parameter, and P is the percent flow parameter.
The transfer volume, D, is corrected to D_{corr} for small transfer volumes:

$$D_{corr} = \ 0\ if\ D < 0.01 \quad (11)$$

Evaporation from open water along the canals is removed from the transfer volume:

$$D_{corr_e} = \begin{cases} D_{corr} - E\ if\ \ (D_{corr} - E) > 0.001 \\ 0 \qquad if\ (D_{corr} - E) \leq 0.001 \end{cases} \quad (12)$$

where D_{corr_e} [m^{3}s^{-1}] is the transfer volume corrected for evaporation, and E [m^{3}s^{-1}] is the evaporation volume:

$$E = L * W * FWE \quad (13)$$

where L [m] is the length of the canal (listed in Table S8 where published data is available, or calculated based on a straight line between to/from points), FWE is free-water evaporation [mm/day] which can be calculated through various free-water evaporation models (42) or by scaled calculated potential evapotranspiration by the Hamon method (43); and W [m] is the width of the canal:

$$W = \begin{cases} \tau * D_{corr}^{\varphi} & if\ (\tau * D_{corr}^{\varphi}) \geq 0.01 \\ 0 & if\ (\tau * D_{corr}^{\varphi}) < 0.01 \end{cases} \quad (14)$$

where τ (8.0) and φ (0.58) are held constant (44).

Water is transferred on a daily time step. Several of the lengthy inter-basin transfers were split into multiple transfer segments for the purpose of the simulation. This allowed for water to be released and/or stored along the canal route, from where it can be accessible for irrigation withdrawals.

C.4. Model Validation

WBM is evaluated by comparing simulated river discharge to the Global Runoff Data Centre [GRDC, 2015] observed discharge. Comparisons are made using the Nash-Sutcliffe efficiency coefficient, NSE [Nash and Sutcliffe, 1970]. See **Figures D1** and **D2** below for a map of global NSE values. WBM river discharge simulations are most accurate in temperate, wet, and northern high-latitude regions. The model is known to under-estimate river discharge in medium-sized basins, as can be seen in **Figure D2.** WBM simulated river discharge is sensitive to climate inputs; see [*Grogan,* 2016] for evaluation and discussion of river discharge simulations using alternative climate inputs. In this study, WBM is used to identify the amount of surface water and ground water available for irrigation. While it is the gridded economic model that simulates changes in future irrigated land and water use, it is important to assess WBM's skill in simulating the distribution of surface vs groundwater use in irrigated areas. **Figure D3** shows good comparison between WBM and FAO-reported (FAO, 2015) country-level statistics on irrigation by water source.

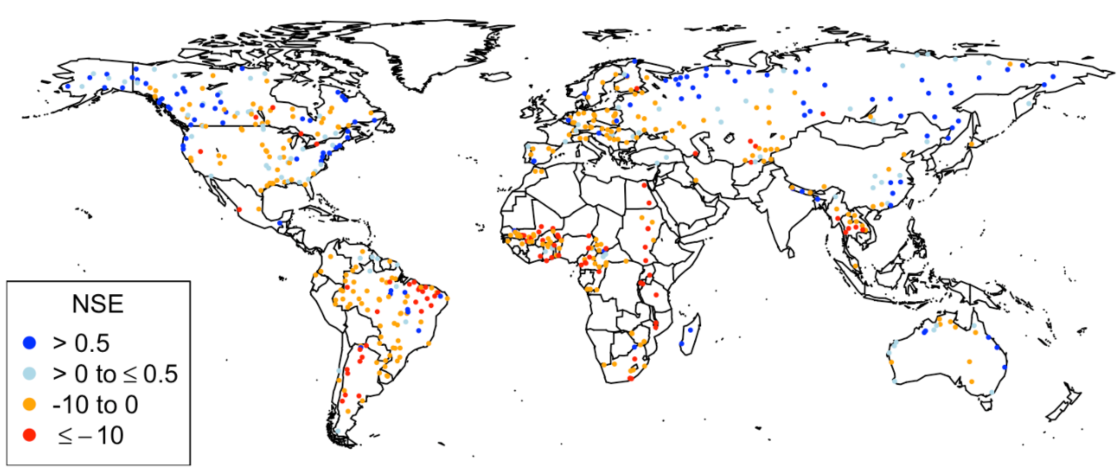

Figure C1. Map of NSE coefficients, comparing WBM-simulated river discharge with global river discharge observations from the GRDC (GRDC, 2015).

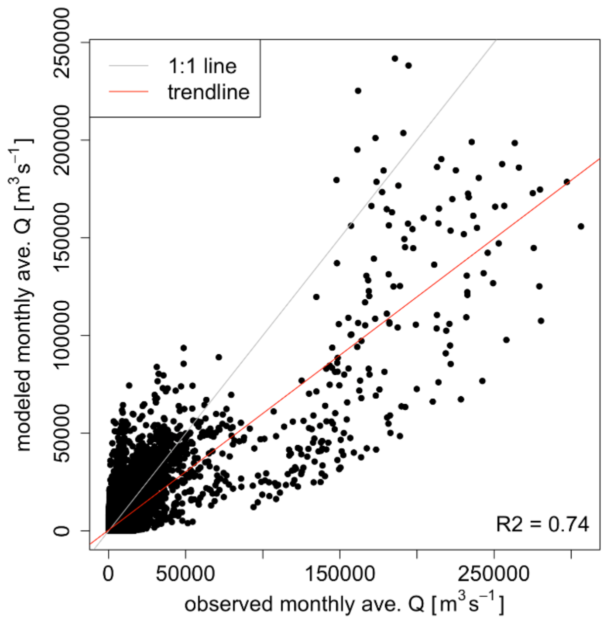

Figure C2. WBM modeled monthly average river discharge (Q), compared to GRDC observed monthly river discharge.

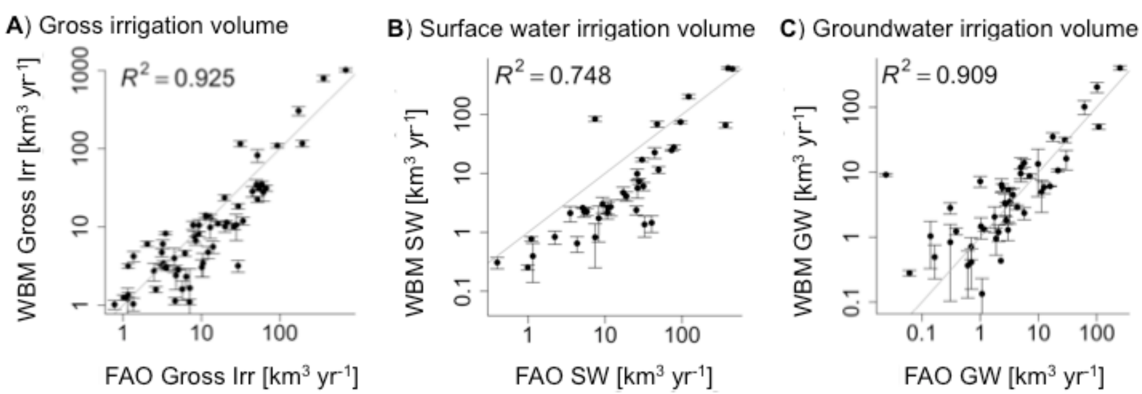

Figure C3. Comparison of country-level WBM-simulated water supplies for irrigation to FAO water supplies for irrigation. Total irrigation water volume is shown in A), surface water is shown in B), and groundwater volume is in C).

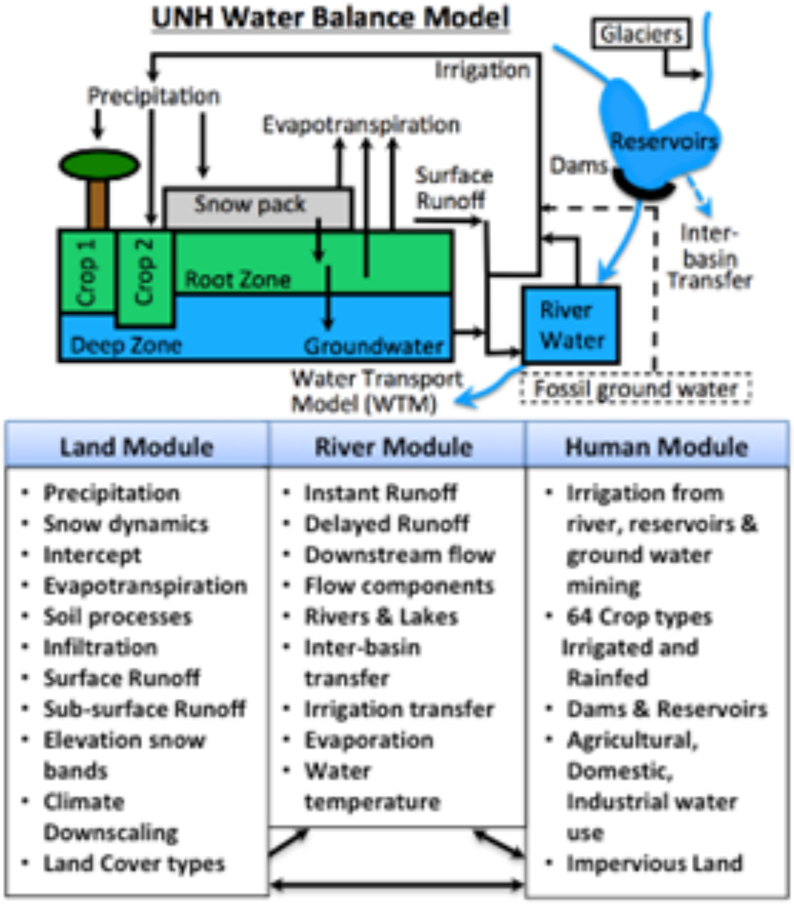

Figure C4. Water Balance Model. Schematic diagram showing major components of the UNH Water Balance Model with a list of processes over the land, river and human interactions.

Appendix D. Summary of the procedure used for downscaling national water use data into grid-cell and projecting future water demand by domestic and industrial sectors. The following equations are for country *N*. Subscript *N* is omitted.

1) Gather base year (2010) national domestic (DWU^{2010}) and industrial (IWU^{2010}) water withdrawal data from FAO
2) Calculate water use intensity (cubic meter per person per GDP dollar) of each, assuming constant intensity over time till year 2100.
   i. Domestic water use intensity,
   $$\eta_D = \frac{DWU^{2010}}{\sum_{g \in N} P_g^{2010} G_g^{2010}} = \frac{DWU^t}{\sum_{g \in N} P_g^t G_g^t}, t = 1980, ..., 2100$$
   ii. Industrial water use intensity, $\eta_I = \dfrac{IWU^{2010}}{\sum_{g \in N} P_g^{2010} G_g^{2010}} = \dfrac{IWU^t}{\sum_{g \in N} P_g^t G_g^t}$
3) Predict national level water use time series, assuming the income elasticity of water demand is 0.2.
   i. Domestic water use, $DWU^t = DWU^{2010}\left[1 + r_{pop}^t + 0.2 \times r_{gpc}^t\right]^{t-2010}$
   ii. Industrial water use, $IWU^t = IWU^{2010}\left[1 + 0.2 \times r_{gdp}^t\right]^{t-2010}$
   iii. Annual growth rate of GDP per capita, $r_{gpc}^t = r_{gdp}^t - r_{pop}^t$
4) Multiply water use intensity with grid-level population and GDP to obtain grid-level water use
   i. $DWU_g^t = \eta_D P_g^t G_g^t$
   ii. $IWU_g^t = \eta_I P_g^t G_g^t$
5) Verify that aggregating grid-level water use gives national water use
   i. $$\sum_{g \in N} DWU_g^t = \sum_{g \in N} \eta_D P_g^t G_g^t = \sum_{g \in N} \frac{DWU^t}{\sum_{g \in N} P_g^t G_g^t} P_g^t G_g^t = DWU^t \sum_{g \in N} \frac{P_g^t G_g^t}{\sum_{g \in N} P_g^t G_g^t} = DWU^t$$
   ii. $$\sum_{g \in N} IWU_g^t = \sum_{g \in N} \eta_I P_g^t G_g^t = \sum_{g \in N} \frac{IWU^t}{\sum_{g \in N} P_g^t G_g^t} P_g^t G_g^t = IWU^t \sum_{g \in N} \frac{P_g^t G_g^t}{\sum_{g \in N} P_g^t G_g^t} = IWU^t$$

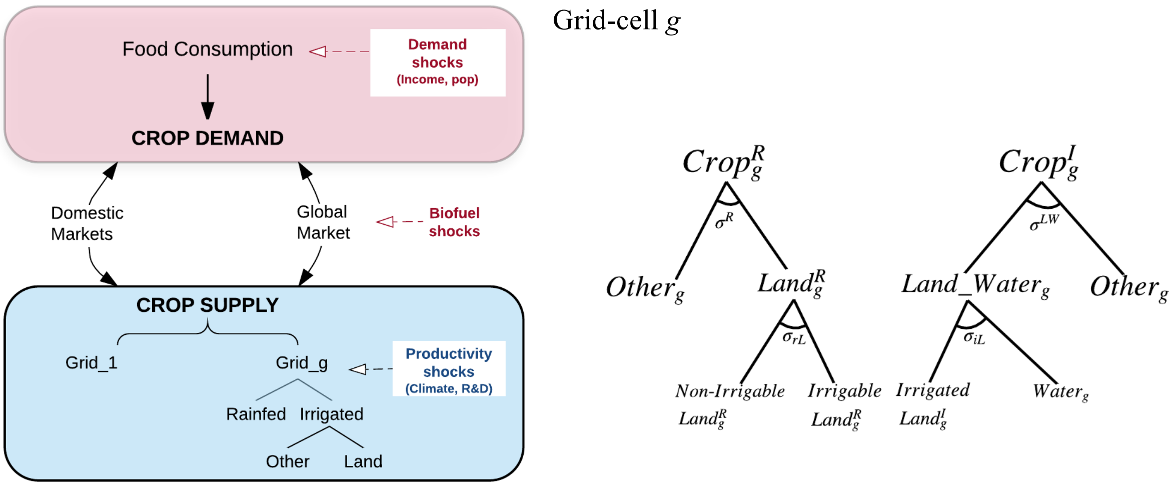

Figure S1. Crop demand and crop supply system in SIMPLE-on-a-Grid model (LHS), and production structure of irrigated and rainfed crop for grid g (RHS). A land-water composite and other non-land inputs are used to produce irrigated crop $Crop_g^I$. The elasticity of substitution between these two inputs is σ^{LW}. Rainfed land $Land_g^R$ and other inputs are used to produced rainfed crop $Crop_g^R$. The elasticity of substitution between rainfed land and other non-land inputs is σ^R. Rainfed land is sourced from non-irrigable land NIL_g^R and irrigable but currently not irrigated land IL_g^R. Non-irrigable land and irrigable land (including both irrigated and irrigable but not irrigated) are subject to different land supply regimes.

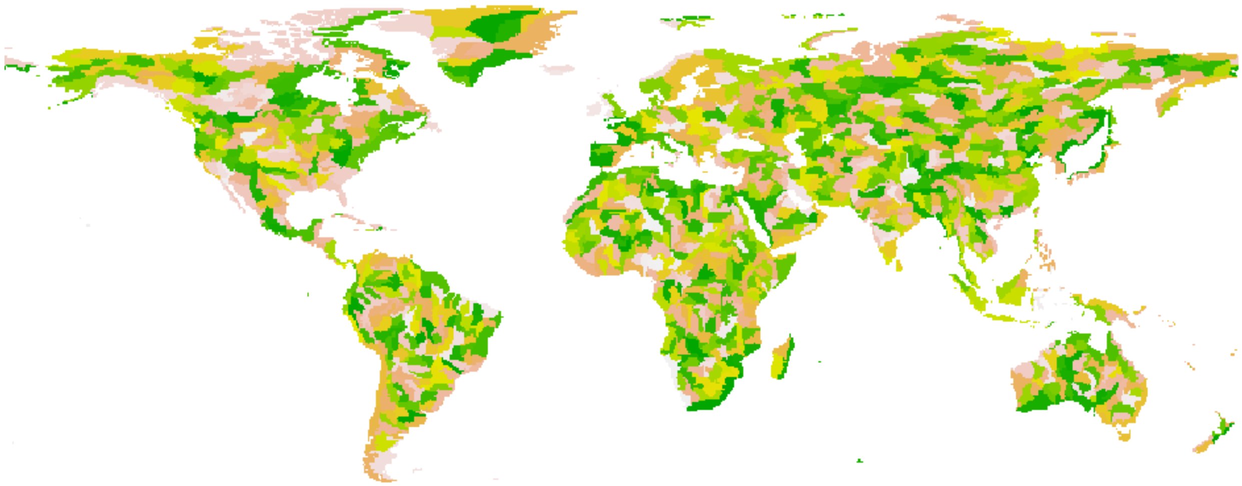

Figure S2. Visualization of the 958 sub-basin regions. Colors are randomly chosen for differentiation purposes.

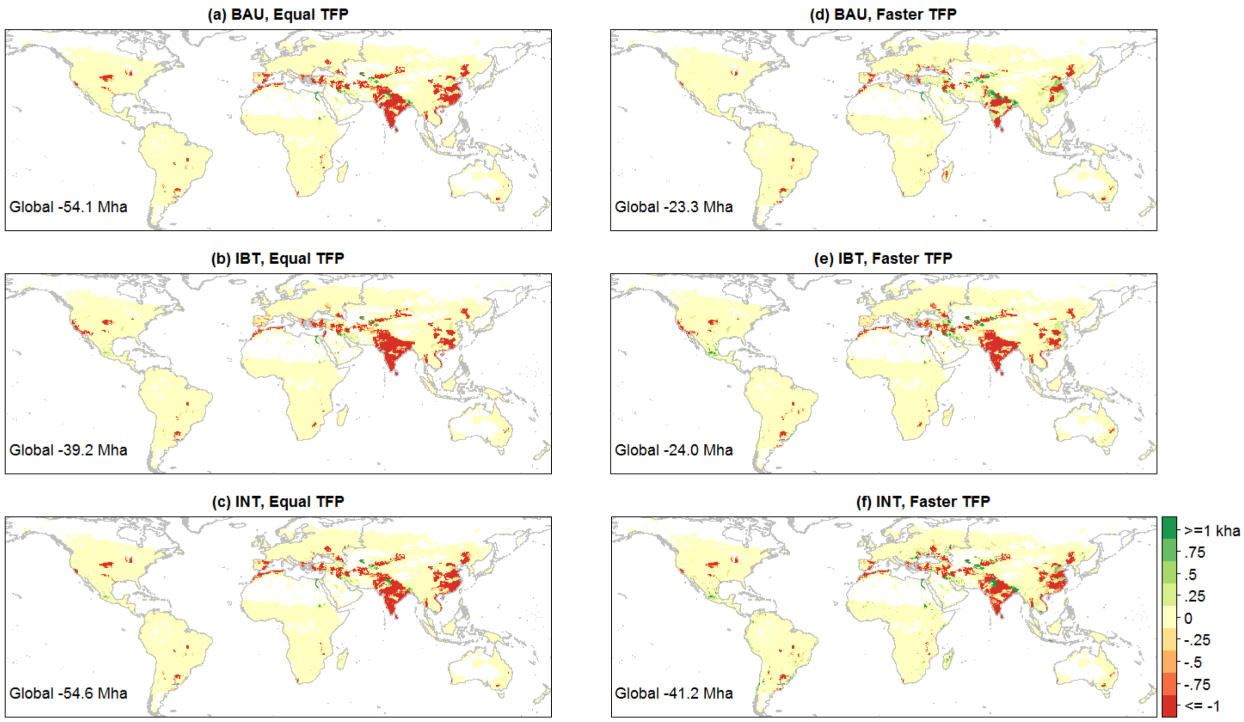

(A)

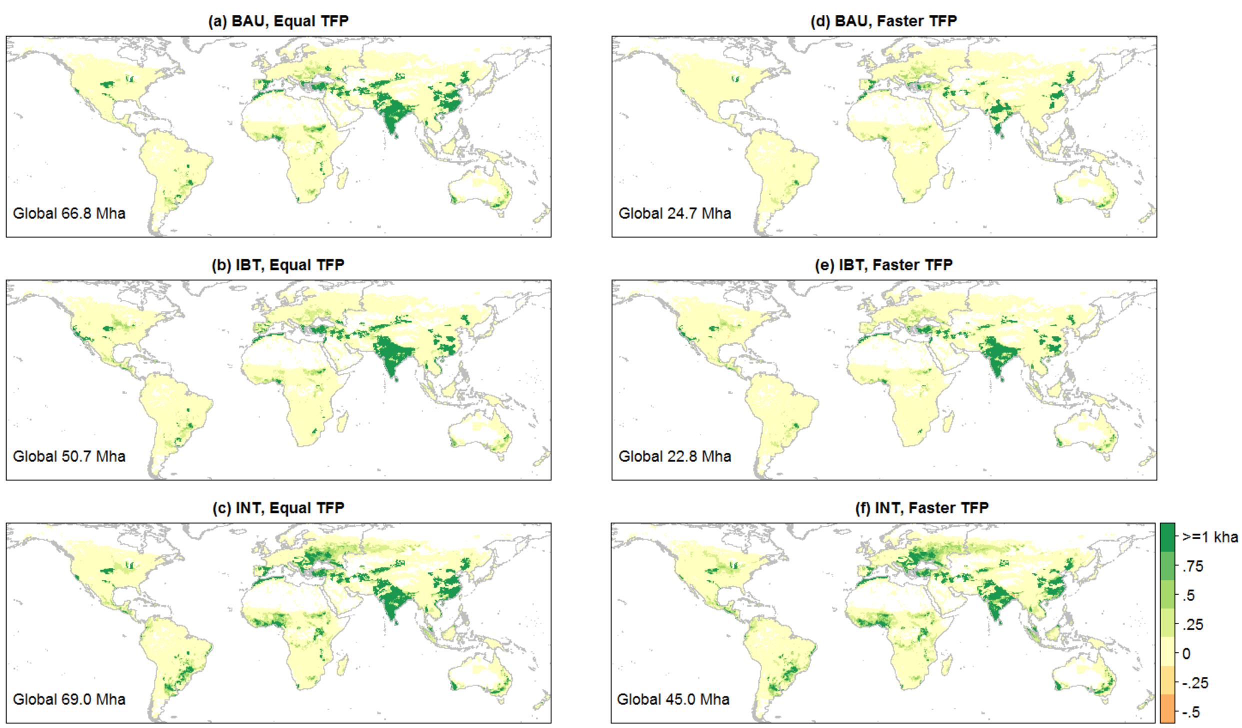

(B)

Figure S3. Irrigated (A) and rainfed (B) cropland area change at the 30 arc-min grid-cell level (unit: thousand hectares).

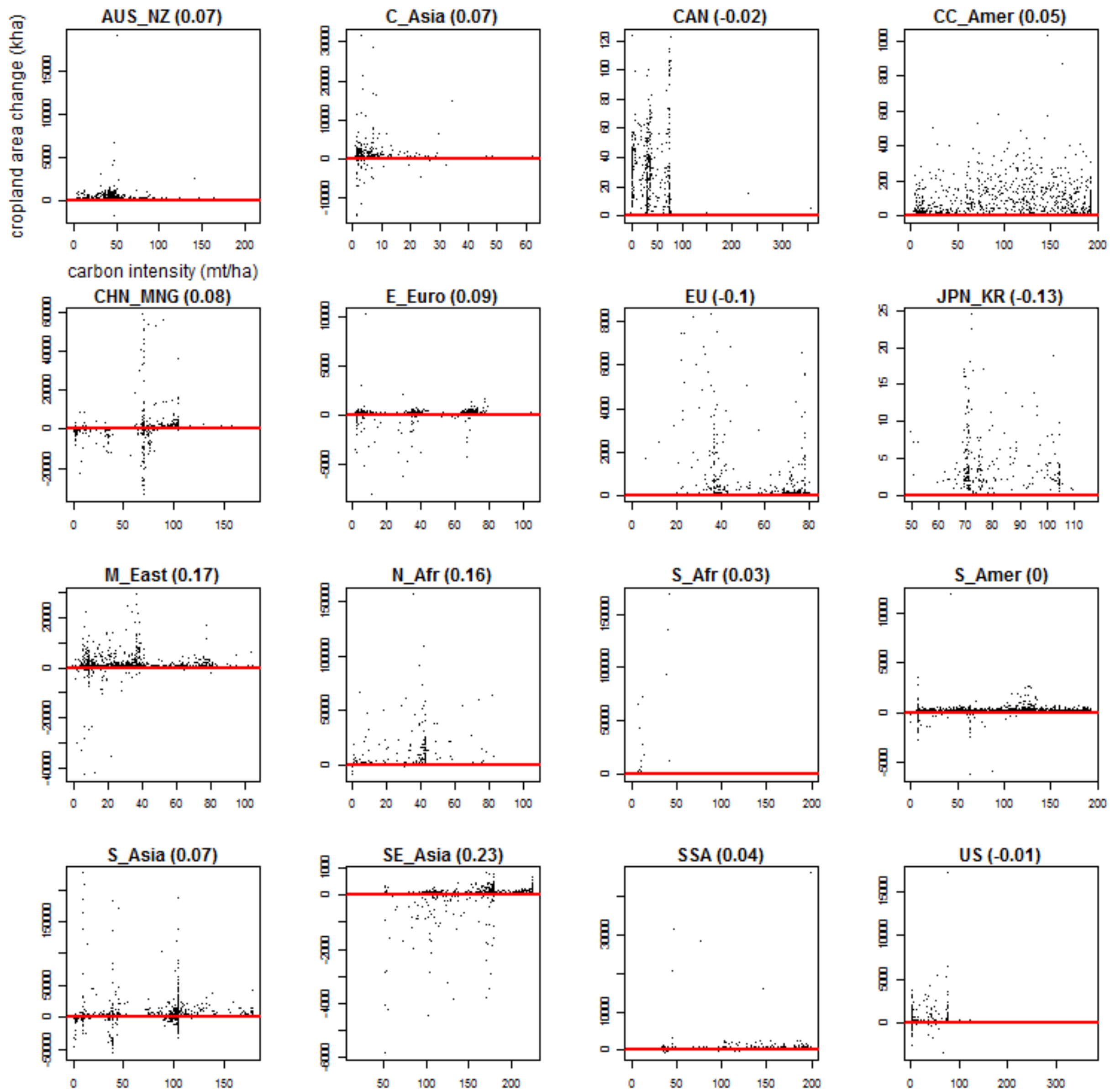

AUS_NZ (0.07)
C_Asia (0.07)
CAN (-0.02)
CC_Amer (0.05)
CHN_MNG (0.08)
E_Euro (0.09)
EU (-0.1)
JPN_KR (-0.13)
M_East (0.17)
N_Afr (0.16)
S_Afr (0.03)
S_Amer (0)
S_Asia (0.07)
SE_Asia (0.23)
SSA (0.04)
US (-0.01)
cropland area change (kha)
carbon intensity (mt/ha)

(A)

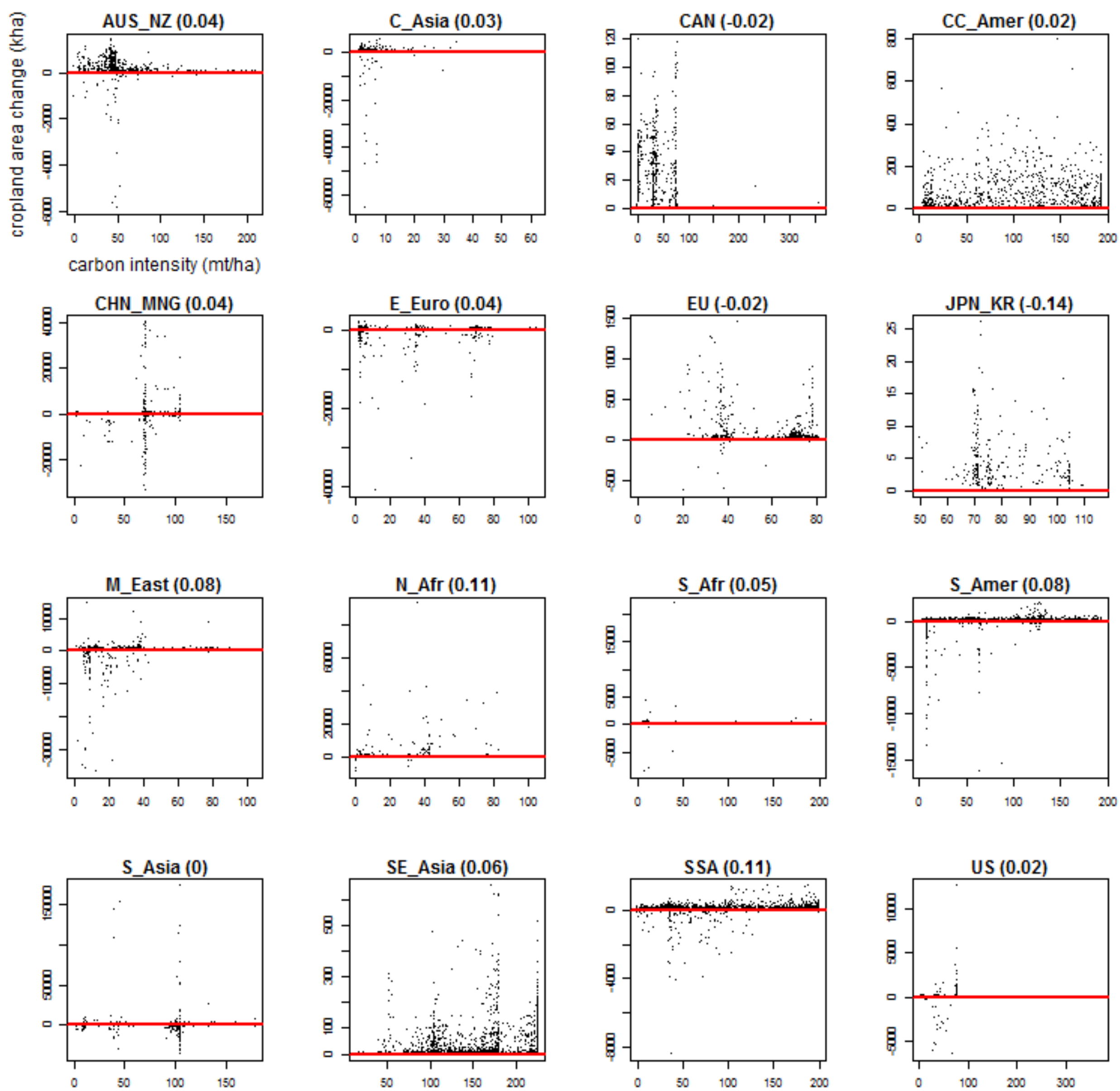

(B)

Figure S4. Spearman correlation plot between grid-level carbon sequestration factor and grid-level net cropland area change. Two experiments are selected to be compared: BAU with equal irrigated TFP growth (A) and BAU with faster irrigated TFP growth (B). Numbers in parenthesis indicate the Spearman correlation coefficient between the carbon intensity and cropland area change. A large positive correlation indicates strong association between cropland expansion and carbon intensity (i.e. more expansion in carbon rich regions). The scatterplots show that even for the same region, cropland area change in each grid (associated with a specific carbon intensity factor) can be different under these two scenarios. Total carbon emissions thus can be different due to the spatial variation.

Table S1. Mapping between SIMPLE-on-a-Grid regions and countries included in the model database

Region	Country (alpha-3 code)
AUS_NZ	aus, nzl
C_Asia	kgz, tjk, tkm, uzb, kaz
CAN	can
CC_Amer	blz, cri, cub, dom, slv, gtm, guy, hti, hnd, mex, nic, pan, pri, sur, tto
CHN_MNG	chn, mng
E_Euro	alb, arm, aze, blr, geo, mda, rom, rus, ukr, ysr, mkd, bih, hrv, svn
EU	aut, bgr, cyp, dnk, est, fin, fra, deu, grc, hun, isl, irl, ita, lva, ltu, nld, nor, pol, prt, esp, swe, che, gbr, bel, lux, cze, svk
JPN_KR	jpn, kor
M_East	irn, irq, isr, jor, lbn, omn, sau, syr, tur, are, yem
N_Afr	dza, egy, lby, mar, tun
SSA	ago, ben, bfa, bdi, cmr, caf, tcd, com, cog, zar, civ, gnq, eri, eth, gab, gmb, gha, gin, gnb, ken, lbr, mdg, mwi, mli, mrt, moz, ner, nga, rwa, sen, sle, tza, tgo, uga, zmb, zwe
S_Afr	bwa, lso, mus, nam, zaf, swz
S_Amer	arg, bol, bra, chl, col, ecu, pry, per, ury, ven
S_Asia	bgd, btn, ind, npl, pak, lka
SE_Asia	khm, fji, idn, lao, mys, png, phl, slb, tha, tmp, vut, vnm
US	usa

Table S2. Model calibration and hindcasting results. The first two columns compare the percentage change of observed and simulated total cropland area in each region from 1961 to 2006. The third column shows the calibrated incremental TFP growth in irrigated crop sector during the same period. The simulated results reasonably follow the observed cropland area change in most major agricultural regions. In the case of the US and the EU, where cropland experiences significant contraction, we attribute this to factors outside this partial equilibrium model and exogenously shift the land supply schedule in order to target total crop land change.

Region	**Observed**	**Simulated**	**Incremental increase in irrigated TFP growth, 1961-2006 cumulated, %**
E_Euro	-24.0	-11.0	3.7
C_Asia	-24.0	-5.0	2.9
EU	-16.6	-16.6	12.0
JPN_KR	-15.7	4.3	9.3
US	-10.0	-10.0	13.3
CAN	-3.8	3.3	14.4
S_Asia	7.1	-0.2	10.3
S_Afr	7.4	-6.9	10.3
M_East	9.8	5.5	13.0
CHN	14.7	9.7	12.3
N_Afr	18.2	15.6	5.5
CC_Amer	23.9	14.4	7.0
AUS_NZ	29.6	6.5	10.5
SE_Asia	35.6	22.9	10.6
SSA	37.1	32.7	4.1
S_Amer	49.1	26.4	2.9
World			8.8

Table S3. Net cropland area change (unit: million hectares) simulated by six experiments.

	Equal irrigated TFP growth			Faster irrigated TFP growth		
Region	BAU	Inter-basin hydrological transfer	Integrated market	BAU	Inter-basin hydrological transfer	Integrated market
S_Asia	5.45	4.30	5.27	0.60	-1.72	0.63
N_Afr	2.92	1.83	2.83	0.84	0.61	1.91
M_East	0.93	1.35	0.89	-0.29	-0.10	-0.58
S_Afr	0.71	0.07	0.68	0.04	-0.02	0.06
CHN	0.67	0.00	0.68	0.30	-0.26	0.00
SSA	0.49	0.24	0.96	0.13	0.21	0.91
C_Asia	0.35	0.27	0.22	-0.38	-0.86	-0.74
EU	0.34	0.12	0.37	0.08	0.04	0.13
AUS_NZ	0.22	0.17	0.31	0.11	0.12	0.28
S_Amer	0.21	0.17	0.64	-0.04	-0.05	0.44
US	0.20	2.71	0.24	0.05	0.86	0.07
E_Euro	0.18	0.15	0.88	-0.18	-0.16	0.21
CC_Amer	0.08	0.17	0.21	0.07	0.11	0.28
CAN	0.02	0.01	0.03	0.02	0.02	0.05
JPN_KR	0.00	0.00	0.00	0.00	0.00	0.01
SE_Asia	-0.02	-0.03	0.11	0.08	-0.04	0.21
World total	12.73	11.52	14.32	1.43	-1.24	3.88

Table S4. Carbon emissions (unit: thousand metric tons of carbon equivalent) simulated by six experiments.

	Equal irrigated TFP growth			**Faster irrigated TFP growth**		
Region	BAU	Inter-basin hydrological transfer	Integrated market	BAU	Inter-basin hydrological transfer	Integrated market
S_Asia	484.15	482.88	466.84	43.96	-72.66	77.54
N_Afr	114.13	71.41	111.26	33.45	23.86	73.87
CHN_MNG	76.13	17.53	80.48	32.76	-11.25	12.90
SSA	54.83	27.01	107.34	19.40	23.39	102.50
M_East	37.36	47.20	35.78	1.75	6.39	-5.94
S_Amer	22.69	19.86	65.33	12.97	15.30	65.05
S_Afr	21.40	2.33	20.75	2.02	-0.86	2.61
EU	15.52	6.57	17.31	4.35	2.34	7.64
AUS_NZ	9.87	7.74	13.73	4.88	5.44	12.31
E_Euro	9.71	7.93	40.77	0.06	1.84	30.21
US	8.63	108.42	10.34	3.48	37.19	7.05
CC_Amer	8.53	21.95	23.12	7.03	24.07	30.81
SE_Asia	4.49	2.29	28.78	15.04	4.18	50.17
C_Asia	2.65	2.01	1.65	-1.61	-6.80	-4.63
CAN	0.55	0.50	1.05	0.53	0.61	1.63
JPN_KR	0.09	0.08	0.28	0.09	0.10	0.45
World total	870.72	825.71	1024.79	180.16	53.15	464.17

References

Baldos, U.L.C., Hertel, T.W., 2013. Looking back to move forward on model validation: insights from a global model of agricultural land use. Environ. Res. Lett. 8, 034024. doi:10.1088/1748-9326/8/3/034024

Dingman, S.L., 2002. Physical hydrology, 2nd ed. Prentice Hall, Upper Saddle River, N.J.

Elvidge, C.D., Tuttle, B.T., Sutton, P.C., Baugh, K.E., Howard, A.T., Milesi, C., Bhaduri, B., Nemani, R., 2007. Global Distribution and Density of Constructed Impervious Surfaces. Sensors 7, 1962–1979. doi:10.3390/s7091962

FAO, 2014. FAOSTAT [WWW Document]. URL http://faostat.fao.org/ (accessed 9.25.14).

FAO/IIASA/ISRIC/ISS-CAS/JRC, 2009. Harmonized world soil database (version 1.1). FAO Rome Italy IIASA Laxenburg Austria Www Doc. URL Httpwww Fao Orgnrlandsoilsharmonized-World-Soildatabaseen.

Federer, C.A., Vörösmarty, C., Fekete, B., 2003. Sensitivity of Annual Evaporation to Soil and Root Properties in Two Models of Contrasting Complexity. J. Hydrometeorol. 4, 1276–1290. doi:10.1175/1525-7541(2003)004<1276:SOAETS>2.0.CO;2

Global Modeling and Assimilation Office (GMAO), 2011. Global Modeling and Assimilation Office (GMAO) and the GES DISC for the dissemination of MERRA.

Grogan, D.S., 2016. Global and regional assessments of unsustainable groundwater use in irrigated agriculture. UNIVERSITY OF NEW HAMPSHIRE.

Grogan, D.S., Zhang, F., Prusevich, A., Lammers, R.B., Wisser, D., Glidden, S., Li, C., Frolking, S., 2015. Quantifying the link between crop production and mined groundwater irrigation in China. Sci. Total Environ. 511, 161–175. doi:10.1016/j.scitotenv.2014.11.076

Hamon, W.R., 1963. Computation of direct runoff amounts from storm rainfall. publisher not identified.

Huffman, G.J., Adler, R.F., Morrissey, M.M., Bolvin, D.T., Curtis, S., Joyce, R., McGavock, B., Susskind, J., 2001. Global Precipitation at One-Degree Daily Resolution from Multisatellite Observations. J. Hydrometeorol. 2, 36–50. doi:10.1175/1525-7541(2001)002<0036:GPAODD>2.0.CO;2

Lehner, B., Liermann, C.R., Revenga, C., Vörösmarty, C., Fekete, B., Crouzet, P., Döll, P., Endejan, M., Frenken, K., Magome, J., Nilsson, C., Robertson, J.C., Rödel, R., Sindorf, N., Wisser, D., 2011. High-resolution mapping of the world's reservoirs and dams for sustainable river-flow management. Front. Ecol. Environ. 9, 494–502. doi:10.1890/100125

Murphy, J.T., Ozik, J., Collier, N., Altaweel, M., Lammers, R.B., Prusevich, A.A., Kliskey, A., Alessa, L., 2015. Simulating regional hydrology and water management: An integrated agent-based approach, in: 2015 Winter Simulation Conference (WSC). IEEE, pp. 3913–3924.

Murphy, J.T., Ozik, J., Collier, N.T., Altaweel, M., Lammers, R.B., Kliskey, A., Alessa, L., Cason, D., Williams, P., 2014. Water Relationships in the U.S. Southwest: Characterizing Water Management Networks Using Natural Language Processing. Water 6, 1601–1641. doi:10.3390/w6061601

Portmann, F.T., Siebert, S., Döll, P., 2010. MIRCA2000—Global monthly irrigated and rainfed crop areas around the year 2000: A new high-resolution data set for agricultural and hydrological modeling. Glob. Biogeochem. Cycles 24, GB1011. doi:10.1029/2008GB003435

Rawlins, M.A., Lammers, R.B., Frolking, S., Fekete, B.M., Vorosmarty, C.J., 2003. Simulating pan-Arctic runoff with a macro-scale terrestrial water balance model. Hydrol. Process. 17, 2521–2539. doi:10.1002/hyp.1271

Schmidt, G.A., Kelley, M., Nazarenko, L., Ruedy, R., Russell, G.L., Aleinov, I., Bauer, M., Bauer, S.E., Bhat, M.K., Bleck, R., Canuto, V., Chen, Y.-H., Cheng, Y., Clune, T.L., Del Genio, A., de Fainchtein, R., Faluvegi, G., Hansen, J.E., Healy, R.J., Kiang, N.Y., Koch, D., Lacis, A.A., LeGrande, A.N., Lerner, J., Lo, K.K., Matthews, E.E., Menon, S., Miller, R.L., Oinas, V., Oloso, A.O., Perlwitz, J.P., Puma, M.J., Putman, W.M., Rind, D., Romanou, A., Sato, M., Shindell, D.T., Sun, S., Syed, R.A., Tausnev, N., Tsigaridis, K., Unger, N., Voulgarakis, A., Yao, M.-S., Zhang, J., 2014. Configuration and assessment of the GISS ModelE2 contributions to the CMIP5 archive. J. Adv. Model. Earth Syst. 6, 141–184. doi:10.1002/2013MS000265

Siebert, S., Döll, P., 2010. Quantifying blue and green virtual water contents in global crop production as well as potential production losses without irrigation. J. Hydrol., Green-Blue Water Initiative (GBI) 384, 198–217. doi:10.1016/j.jhydrol.2009.07.031

UN Population Division, 2015. World Population Prospects: The 2015 Revision. Population Division of the Department of Economic and Social Affairs of the United Nations Secretariat, New York , USA.

Vörösmarty, C.J., Federer, C.A., Schloss, A.L., 1998. Potential evaporation functions compared on US watersheds: Possible implications for global-scale water balance and terrestrial ecosystem modeling. J. Hydrol. 207, 147–169. doi:10.1016/S0022-1694(98)00109-7

Vörösmarty, C.J., Fekete, B.M., Meybeck, M., Lammers, R.B., 2000. Geomorphometric attributes of the global system of rivers at 30-minute spatial resolution. J. Hydrol. 237, 17–39. doi:10.1016/S0022-1694(00)00282-1

Vörösmarty, C.J., McIntyre, P.B., Gessner, M.O., Dudgeon, D., Prusevich, A., Green, P., Glidden, S., Bunn, S.E., Sullivan, C.A., Liermann, C.R., Davies, P.M., 2010. Global threats to human water security and river biodiversity. Nature 467, 555–561. doi:10.1038/nature09440

Wisser, D., Fekete, B.M., Vörösmarty, C.J., Schumann, A.H., 2010. Reconstructing 20th century global hydrography: a contribution to the Global Terrestrial Network- Hydrology (GTN-H). Hydrol Earth Syst Sci 14, 1–24. doi:10.5194/hess-14-1-2010

Wisser, D., Frolking, S., Douglas, E.M., Fekete, B.M., Schumann, A.H., Vörösmarty, C.J., 2010. The significance of local water resources captured in small reservoirs for crop production – A global-scale analysis. J. Hydrol., Green-Blue Water Initiative (GBI) 384, 264–275. doi:10.1016/j.jhydrol.2009.07.032

Wisser, D., Frolking, S., Douglas, E.M., Fekete, B.M., Vörösmarty, C.J., Schumann, A.H., 2008. Global irrigation water demand: Variability and uncertainties arising from agricultural and climate data sets. Geophys. Res. Lett. 35, L24408. doi:10.1029/2008GL035296

Wisser, D., Frolking, S., Hagen, S., Bierkens, M.F.P., 2013. Beyond peak reservoir storage? A global estimate of declining water storage capacity in large reservoirs. Water Resour. Res. 49, 5732–5739. doi:10.1002/wrcr.20452

Wollheim, W.M., Vörösmarty, C.J., Bouwman, A.F., Green, P., Harrison, J., Linder, E., Peterson, B.J., Seitzinger, S.P., Syvitski, J.P.M., 2008. Global N removal by freshwater aquatic systems using a spatially distributed, within-basin approach. Glob. Biogeochem. Cycles 22, GB2026. doi:10.1029/2007GB002963

World Development Indicators, 2015. . World Bank, Washington, D.C., USA.

Zaveri, E., Grogan, D.S., Fisher-Vanden, K., Frolking, S., Lammers, R.B., Wrenn, D.H., Prusevich, A., Nicholas, R.E., 2016. Invisible water, visible impact: groundwater use and Indian agriculture under climate change. Environ. Res. Lett. 11, 084005.